

Submitted to Journal of the
Optical Society of America

RECEIVED
LAWRENCE
RADIATION LABORATORY

LBL-1102
Preprint

NOV 20 1972

LIBRARY AND
DOCUMENTS SECTION

LIGHT DEFLECTION EFFECTS IN THE INTERFEROMETRY
OF ONE-DIMENSIONAL REFRACTIVE INDEX FIELDS

K. W. Beach, R. H. Muller and C. W. Tobias

September 1972

AEC Contract No. W-7405-eng-48

For Reference

Not to be taken from this room



LBL-1102

DISCLAIMER

This document was prepared as an account of work sponsored by the United States Government. While this document is believed to contain correct information, neither the United States Government nor any agency thereof, nor the Regents of the University of California, nor any of their employees, makes any warranty, express or implied, or assumes any legal responsibility for the accuracy, completeness, or usefulness of any information, apparatus, product, or process disclosed, or represents that its use would not infringe privately owned rights. Reference herein to any specific commercial product, process, or service by its trade name, trademark, manufacturer, or otherwise, does not necessarily constitute or imply its endorsement, recommendation, or favoring by the United States Government or any agency thereof, or the Regents of the University of California. The views and opinions of authors expressed herein do not necessarily state or reflect those of the United States Government or any agency thereof or the Regents of the University of California.

LIGHT DEFLECTION EFFECTS IN THE INTERFEROMETRY OF
ONE-DIMENSIONAL REFRACTIVE INDEX FIELDSK. W. Beach,^{*} R. H. Muller and C. W. TobiasInorganic Materials Research Division, Lawrence Berkeley Laboratory
and Department of Chemical Engineering; University of California
Berkeley, California

ABSTRACT

Distortions in interferograms of refractive index fields due to deviations from straight-line light propagation have been analyzed numerically. It is shown that quantitative refractive index profiles can often not be derived in a simple way from interferograms. The choice of the plane of focus and the alignment of the object with respect to the light direction are found to greatly affect the distortions. Results for typical examples of refractive index fields encountered in different electrochemical systems are given.

* Present address: School of Medicine, University of Washington, Seattle, Washington. 98195

LIGHT DEFLECTION EFFECTS IN THE INTERFEROMETRY
OF ONE-DIMENSIONAL REFRACTIVE INDEX FIELDS

Optical interferometry has long been used for the observation of refractive index fields.¹⁻⁷ The conventional interpretation of the resulting interferograms is based on the assumption that light propagates along a straight line through the specimen. Local variations in the phase of light transmitted through a specimen of uniform dimension are then taken as a direct measure of local refractive index variations. The presence of refractive index variations normal to the light propagation direction results, however, in a deviation from straight-line propagation. This phenomenon is unavoidably associated with light transmission through media of locally varying refractive index and forms the basis of Schlieren-optical techniques.^{8,9}

Light deflection can be expected to result in two kinds of errors in an interferogram. The first is a geometrical distortion (displacement of the virtual beam origin) due to the lateral displacement and change in direction of transmitted light. The second is a distortion of the apparent local refractive index (error in phase) due to the increased geometrical path length and passage through different regions of the specimen.

In the present paper, errors due to light deflection in the quantitative interpretation of interferograms are examined. Computational techniques have been developed to account for these errors in one-dimensional refractive index fields, as they are encountered in the double beam interferometry of electrolytic mass transfer boundary layers¹⁰ and other diffusion or separation processes in liquid media.^{1,11} The approach

can be modified for use with multiple beam interferograms and two or three-dimensional refractive index fields.

LIGHT DEFLECTION DUE TO REFRACTIVE INDEX GRADIENTS

Light deflection in media of locally varying refractive index has traditionally been treated in connection with Schlieren-optical applications.^{2,9} Recent interest in this topic is mostly due to the use of inhomogeneous media for imaging devices.¹²⁻¹⁵

Attempts to calculate light deflection errors in interferograms have been reported by several authors.^{2,10,11,16,17} In some cases, errors have been found negligible, a conclusion which appears valid only for gaseous media^{5,16} or small refractive index variations at a large distance from the camera.¹⁸ The effect of the imaging optics on the interferogram,^{11,17,18} even where it has been considered, has not been sufficiently analyzed.

The physical reason for light deflection (or refraction) in refractive index fields lies in the dependence of propagation velocity on refractive index n . If different elements of a wavefront W_1 (Fig. 1) advance at different rates, a tilted wavefront W_2 results after a distance dx is traversed. Correspondingly, the original propagation direction, indicated by the wave normal N_1 is changed to N_2 . For an original propagation direction parallel to the x -axis and a refractive index varying in the y -direction the incremental deflection angle is,^{9,11}

$$\frac{dy}{dx} = \frac{1}{n} \frac{dn}{dy} dx \quad (1)$$

For a general propagation direction with respect to coordinate system and refractive index gradient, a coordinate rotation¹⁹ of Eq. (1) results in¹³

$$\frac{d^2 y}{dx^2} = \frac{1}{n(x,y)} \left(1 + \left(\frac{dy}{dx} \right)^2 \right) \left(\frac{\partial n}{\partial y} - \frac{\partial n}{\partial x} \left(\frac{dy}{dx} \right) \right) \quad (2)$$

For a three-dimensional refractive index field, Eq. (3) is derived similarly

$$\frac{d^2 z}{dx^2} = \frac{1}{n(x,y,z)} \left(1 + \left(\frac{dz}{dx} \right)^2 \right) \left(\frac{\partial n}{\partial z} - \frac{\partial n}{\partial x} \left(\frac{\partial z}{\partial x} \right) \right) \quad (3)$$

The optical path length p of a deflected beam is

$$p = \int_0^x n(x,y) \left(1 + \left(\frac{dy}{dx} \right)^2 \right)^{1/2} dx \quad (4)$$

Its phase is obtained by division with the vacuum wavelength λ_0

$$\phi = \frac{p}{\lambda_0} 2\pi \quad (5)$$

For some specific refractive index profiles, closed-form solutions for the light path are available.^{10,15,16,20,21} A detailed analysis of light deflection in constant refractive index gradients normal to the original beam direction has been given elsewhere.²²

EFFECT OF FOCUSING

The purpose of the imaging optics in an interferometer is to bring a selected plane in the object to focus in the image. The object plane, which is optically conjugate to the image plane, will be referred to in the following as "plane of focus", but should not be confused with the planes which contain the primary and secondary focal points of the objective lens. If light deflection occurs in the object, the image is determined by the virtual origin of the deflected light in the plane of focus. Under these circumstances the shape of the image can be expected to depend on the choice of the plane of focus. This effect is illustrated in Fig. 2 for a cathodic boundary layer²³ with the electrode shadow as the object. A light beam C, entering the cell at the surface of electrode B and parallel to it, is deflected toward the bulk of the solution A and leaves the cell at point D. With the objective lens G focused on the cell wall facing the camera (Fig. 2a), the shadow of the cathode surface in this plane appears at D and its image in film plane I is H. Thus, the electrode shadow appears advanced into the solution side of the interface because of the presence of the refractive index gradient. Focusing on the cell wall facing the light source (Fig. 2c) results in a virtual origin L of the same deflected beam. The electrode shadow now appears receded into the electrode. For an intermediate focusing position (Fig. 2b), the virtual origin K of the deflected beam coincides with the electrode surface. The electrode shadow is, therefore, not displaced in the image.

In the schematic of Fig. 2, refraction at the interfaces which the light traverses upon leaving the cell has been neglected. Even in the

absence of refractive index gradients, these effects result in an axial displacement of the virtual location E' of an immersed object E (Fig. 3). Since refraction in the first cell wall (even if the incidence was not normal) does not affect image geometry, refraction in the second one only (facing the camera) will be considered.

The application of Snell's law results in Eq. (6) for the virtual location m of an immersed object (Fig. 3).

$$m = \cot \eta (w \tan \epsilon + d \tan \epsilon') \quad (6)$$

For small angles ϵ from the optical axis, this equation reduces to

$$m = \frac{w}{n} + \frac{d}{n_g} \quad (7)$$

As indicated in Fig. 3, w is the thickness of the medium of refractive index n and d is the thickness of the glass wall of refractive index n_g . Thus, a real plane of focus F inside the cell is transformed into a virtual plane of focus F' by refraction effects. (F' would be the real plane of focus in the absence of the cell.) If the imaging optics of an interferometer are focused on an immersed target in plane F , the image is determined by the virtual location of the target in plane F' .

The effect of focusing in the presence of light deflection with consideration of refraction in cell wall and at cell exit is illustrated in Fig. 4 for an arbitrary plane of focus F in the cell (with associated virtual plane of focus F'). A deflected light beam ABC appears to originate from point E' with a lateral displacement g from its true origin A .²⁴ It can be seen that this displacement of the virtual beam origin, which results in a geometrical distortion of the image, strongly

depends on the location of the plane of focus, as it does on the refractive index gradient. The displacement can assume values comparable to the dimension of typical mass transfer boundary layers. Because the virtual plane of focus F' is shifted by changes in cell wall thickness, the beam displacement g is independent of wall thickness (within the approximations of Eq. (7)) for a given choice of the plane of focus F .

For cathodic boundary layers, with refractive index increasing from the interface toward the bulk solution, differently deflected beams may cross each other near the light exit side of the cell (Fig. 5). Ambiguities in the interferogram due to the superposition of differently deflected light can be avoided by use of a plane of focus near the light entrance side of the cell, so that the virtual origins of different rays in the virtual plane of focus F' do not overlap. Scribed lines on the inside face of the cell wall away from the camera have been successfully used to precisely establish such a plane of focus.

The error in phase due to light deflection can be represented by the difference in optical path length between a deflected beam AC (Fig. 6) and a hypothetical undeflected beam EI passing through the same virtual origin E' in the virtual plane of focus. Points C and I lie on a circle entered in E' . Beyond points C and I , the imaging optics introduce no phase difference between the two beams. It will be seen that the error in phase strongly depends on the location of the plane of focus. The error can be of the same magnitude as the phase change expected without light deflection. The thickness of the glass wall has been found to have almost no effect on phase.

Boundary layers with refractive index increasing toward the electrode surface, such as those typically encountered in anodic metal dissolution,

cause the light to be deflected toward the electrode. If all the light which strikes the electrode surface is absorbed, rays entering the cell closer to the electrode than a critical distance do not contribute to the image (Fig. 7b). In contrast to the cathodic boundary layers, an overlapping of the virtual origins of differently deflected beams is now best avoided by focusing on the plane where the light leaves the cell. If the electrode is sufficiently smooth, light which strikes the surface may be reflected (Fig. 7c), and a much more complex optical situation exists, particularly if a reflected beam is deflected back to the electrode surface and reflected again.

The effect of focusing with other refractive index configurations needs to be examined for each specific case. Some examples are given in a later section.

COMPUTATION OF INTERFERENCE FRINGES

In order to compute an interferogram for a given refractive index field, Eqs. (2) and (4) have been solved numerically and the effects of focusing have been incorporated in the analysis.²⁵ The optical paths of 50-100 beams, which enter the cell parallel to each other, usually parallel to the electrode surface, and with 0.04 mm increment in distance from the electrode, have been determined. Each beam is divided into a large number (100-200) of straight segments, as schematically shown in Fig. 8b. The slope of a typical segment HJ is determined from the slope of the previous segment, the length of the segment, the refractive index n_h in the region (Fig. 8a) and the component of the local refractive index gradient in the direction normal to the beam.

The optical path length of a deflected beam, including refraction KL in the cell wall, is obtained by summing the product of local refractive index n_h and geometrical path length HJ of each beam element. From position and slope of the beam M leaving the cell, the virtual origin E' of the deflected beam in the virtual plane of focus is determined. The fringe shift in the interferogram relative to the bulk solution is due to the difference in optical path length between deflected beam GL and a hypothetical undeflected beam EO of the same virtual origin E', passing through a cell filled with bulk solution. Thus, phase and position of one point in the interferogram have been established. Repetition of this procedure with 50-100 beams yields a computed interference fringe.

Figure 9 illustrates how the above procedure can provide computed

interference fringes B to E for an assumed refractive index profile A with different choices of plane of focus. It can be seen that both boundary layer thickness and interfacial concentration are seriously falsified by the light deflection, and the error strongly depends on the choice of the plane of focus. A common observation with such computed interference fringes is that the location of the outside edge of the boundary layer is not affected by light deflection. An exception is seen in Fig. 9e, where a double value of phase is due to the superposition of differently deflected rays in the image.

An experimental observation of the effect of the choice of plane of focus on the appearance of the interferogram is illustrated in Fig. 10. The dependence of apparent boundary layer thickness and interfacial concentration on focus agrees qualitatively with the computations for a slightly different situation given in Fig. 9. The double value of phase, seen in Fig. 9e seems to be responsible for the extraneous interference fringe systems seen in Fig. 10c and 10d. More detailed, quantitative experimental tests of the theoretical analysis are in progress. A displacement of the electrode shadow at high current densities has also been observed by Tvarusko and Watkins.²⁶

DISPLAY OF COMPUTED LIGHT PATH

A display of a small number of the ray tracings computed by the above method has been found helpful in understanding computed interference fringes. The left hand side of Fig. 11 shows the refractive index profile and a computed interference fringe. The short lines between the two curves connected points in the image with the corresponding entering beams. The right-hand side of Fig. 11 shows ray tracings in a cross section of the cell. The air space and glass wall on the light entrance side of the cell are omitted. Figure 11 illustrates that the reason why interference fringes in the boundary layer considered in Fig. 9 nearly vanish for focusing near the light exit side of the cell is that most of the deflected rays converge in this region. It is also shown that, under the conditions of Fig. 11, most of the light is deflected out of the boundary layer before it leaves the cell. (Due to the different scales employed for horizontal and vertical direction in the ray tracings, light deflection angles appear enlarged.)

EXAMPLES OF COMPUTATIONS

Because of the large number of variables and non-linear effects involved in the numerical analysis of light deflection in refractive index fields, it is difficult to generalize results. The analysis can easily be adapted to investigate the effect of additional parameters on the interferogram. For instance, the effect of misalignment of the cell, with the incident light not parallel to the electrode surface has been studied.

In the following, representative examples of theoretical interference fringes and ray tracings will be shown.²⁵ They have all been derived for a cell width (dimension in the beam direction) of 10 mm and a glass wall thickness of 12.7 mm. The liquid medium is a 0.1 M aqueous copper sulfate solution. Concentration C (moles/liter) and refractive index n have been assumed to be correlated by Eq. (8)

$$n = 1.3313 + 0.027952 C \quad (8)$$

Concentration profile and interference fringe for focusing according to case B below are shown with the ray tracings. The interference fringes B to E for refractive index profile A pertain to the following choices of plane of focus

- B - inside face of glass wall far from camera
- C - 1/3 the way across the cell from B
- D - 2/3 the way across the cell from B
- E - inside face of glass wall near camera

Cathodic Boundary Layers

The observation of electrochemical boundary layers by optical interferometry¹⁰ offers the possibility to determine the local rate of mass transfer under conditions which are not restricted to operation at limiting current.²⁷ Cathodic metal deposition from aqueous solutions has been used by several investigators^{26,28-30} as a model for interferometric mass transfer studies.

Figure 12 demonstrates that the thickness of the glass wall has a very small effect on the interference pattern of a cathodic boundary layer under any of the focusing conditions B to E.

Misalignment of the cell by $+2.3^\circ$ (light directed away from electrode face) drastically affects the appearance of interference fringes, as shown in Fig. 13 by comparison with Fig. 12a. The apparent interfacial concentration is increased. The opposite usually holds for misalignment in the other (negative) direction, unless the light is directed toward the electrode surface at such a high angle that much of the light which has passed through the boundary layer strikes the surface, and is (assumed) absorbed (Fig. 14). The apparent concentration maximum, which becomes visible under the conditions employed in Fig. 14, may be compared to a true maximum of hydrodynamic origin described before.²⁸ Compared to the previous observation, the present maximum is broader and not adjacent to a minimum.

Alignment of the cell wall normal to the incident light has been accomplished by directing the reflection from the wall to coincide with the incident beam.

Anodic Boundary layers

Anodic dissolution boundary layers, with refractive index increasing toward the interface, cause light deflection toward the interface. Changes in the appearance of interference fringes with changing focus are similar to the cathodic case, except that focus on the cell exit now produces the least distorted interference fringe (Fig. 15). In this case, the apparent boundary layer thickness is not distorted, but the interfacial concentration seems too low because the deflected ray which leaves the cell at the electrode surface has traveled mostly through the outer parts of the boundary layer, where concentrations are lower than at the interface.

If one attempts to compensate for light deflection in an anodic boundary layer by directing the incident light away from the interface (positive angle of incidence) an apparent concentration minimum may occur (Fig. 16) analogous to the maximum found in the cathodic case (Fig. 14).

Liquid Junctions

In the determination of diffusion coefficients by interferometry, the boundary between two solutions of different concentration is observed. As illustrated in Fig. 17, light deflection causes only minor distortions of such a boundary. Focusing 0.33 cm from the inside face of the glass wall facing the camera (position D) provides the least distortion. Off-axis illumination of the same diffusing boundary causes serious distortions with the appearance of false concentration extrema (Fig. 18). Misalignment in the opposite direction is found to have even more severe effects.

Concentration Minima

Real refractive index extrema can occur in electrophoresis, electro dialysis and after an electrolysis current is reversed. A local refractive index minimum with moderately steep flanks is best observed with the plane of focus at the light-exit side of the cell (position E, Fig. 19). Since the light is deflected from the center of the minimum to both sides, the intensity of the experimental light beam is decreased in the center region and the contrast of interference fringes may be reduced to the point where they disappear. Off-axis light incidence leads to asymmetric distortions with the appearance of false concentration extrema similar to those computed for a liquid junction (Fig. 18).

Concentration Maxima

Light rays converge on a refractive index maximum. If only small gradients and thin cells are involved, focusing on the cell wall away from the camera provides interference fringes with little distortion.

A refractive index maximum with steep flanks results in fringe cross-over regardless of the choice of focal plane (Fig. 20). Under even more severe conditions the light may zigzag across the maximum.²¹

DETERMINATION OF REFRACTIVE INDEX PROFILES FROM INTERFEROGRAMS

For the quantitative interpretation of measured interference fringes as refractive index profiles, the computational methods described are employed in an iterative process. First, an approximate refractive index profile is derived from the observed interferogram. Interference fringes are then computed for the approximate refractive index profile, under consideration of focusing, cell dimension and orientation. Based on a comparison of observed and computed interference fringes, the approximate refractive index profile is subsequently modified to improve agreement between the two. Several cycles are usually necessary to produce satisfactory agreement.

CONCLUSIONS

The present analysis shows that the determination of concentration profiles in liquids by interferometry is often not as straightforward, as has commonly been assumed. Light deflection effects rapidly increase with increasing cell dimension (in the direction of light propagation) and refractive index gradient. In order to account for light deflection, the following points must be considered in the operation of an interferometer:

1. The location of the plane of focus must be established accurately. Locations which minimize ambiguities due to the superposition of differently deflected light should be chosen (summarized in Table I).
2. The alignment of the refractive index field with respect to the direction of the entering light must be known precisely. Usually, the incoming beam should be normal to the refractive index gradient (or cell wall).

Table I. Preferred location of the plane of focus for different refractive index fields

Field	Location
Cathodic boundary layer	Cell wall away from camera
Anodic boundary layer	Cell wall close to camera
Liquid junction	Center of cell
Concentration minimum	Cell wall close to camera
Concentration maximum (small gradients and thin cells only)	Cell wall away from camera

3. The aperture of the imaging optics in the interferometer must be large enough to accept the most deflected light.

With the preferred focusing and light incidence, regions of vanishing refractive index gradient are imaged in their correct position. False maxima, minima and phase boundary positions can often be identified by varying plane of focus and angular alignment.

The effect of refractive index gradients in the direction of light propagation can be incorporated in the computational procedure. Unless such refractive index variations can be inferred on the basis of symmetry considerations,^{5,15} their determination requires additional measurements, one of which has been suggested elsewhere.³¹

The determination of a refractive index immediately adjacent to a phase boundary (e.g., electrode surface) is further limited by diffraction effects which require separate consideration.

ACKNOWLEDGEMENT

This work was conducted under the auspices of the U. S. Atomic Energy Commission.

REFERENCES AND NOTES

1. L. G. Longworth, *Anal. Chem.* 23, 346 (1951).
2. F. J. Weinberg, *Optics of Flames*, (Butterworths, London, 1963).
3. R. B. Kennard, *J. Research* 8, 787 (1932).
4. R. L. Rowe, *ISA Trans.* 5, 44 (1966).
5. J. Winckler, *Rev. Sci. Instr.* 19, 307 (1948).
6. H. J. Raterink and C. W. Samberts, in *Proc. 9th Int. Congress on High-Speed Photography*, W. Hyzer and W. G. Chace, eds. (Soc. Motion Picture and Television Engrs., New York, 1970).
7. T. Zobel, *Z. Verein Deutscher Ing.* 81, 619 (1937).
8. H. Schardin, in *Ergebn. exakt. Naturwiss.*, F. Hund and F. Trendelenburg, eds. (Springer Verlag, Berlin, 1942) Vol. 20, p. 303.
9. H. Wolter, in *Encyclopedia of Physics*, S. Fluegge, ed., (Springer Verlag, Berlin, 1956) Vol. 24.
10. N. Ibl, *Proc. 7th Meeting Int. Comm. Electrochem. Thermodynamics and Kinetics*, Lindau 1955 (Butterworths Publ., London, 1957) p. 112.
11. L. T. Gosting, in *Adv. Protein Chem.* 11, 429 (1956).
12. E. G. Rawson, D. R. Herriott and J. McKenna, *Appl. Optics* 9, 753 (1970).
13. F. P. Kapron, *J. Opt. Soc. Am.* 60, 1433 (1970).
14. W. Streifer and K. B. Paxton, *Appl. Optics* 10, 769 (1971).
15. E. W. Marchand, *J. Opt. Soc. Am.* 60, 1 (1970).
16. P. A. Gooderum, G. P. Wood and M. J. Brevoort, 36th Ann. Report National Advisory Comm. Aeronautics (U. S. Government Printing Office, 1951, Report 963) p. 289.
17. H. Svensson, *Optica Acta* 1, 25 (1954).

18. E. Calvert and R. Chevalerias, J. de Chim. Phys. 43, 37 (1946).
19. K. W. Beach, A Laser Interferometer for Mass Transfer Studies, Dept. of Chemical Engineering, U. C. Berkeley, (M.S. Thesis) UCRL-18037, Feb. 1968.
20. E. v. Heydebrand und der Lasa, Ann. Physik [5] 37, 589 (1940).
21. W. H. Southwell, J. Opt. Soc. Am. 61, 1715 (1971).
22. R. H. Muller, in Advances in Electrochemistry and Electrochemical Engineering, R. H. Muller, ed. (Interscience, New York) Vol. 9 (in press).
23. A cathodic boundary layer in electrolysis is a depleted (lower refractive index) region of solution near the electrode on which a solute is removed from the solution, such as e.g., in the cathodic deposition of copper from a copper sulfate solution. Conversely, an anodic boundary layer, in this context, denotes a region of increased interfacial concentration (or refractive index) relative to the bulk liquid.
24. Because light deflection results in a lateral shift of the sample beam with respect to the reference beam, sufficient lateral coherence is necessary to maintain good fringe contrast.
25. K. W. Beach, Optical Methods for the Study of Convective Mass Transfer Boundary Layers on Extended Electrodes, Dept. of Chemical Engineering, U. C. Berkeley (Ph. D. Thesis) UCRL-20324, June 1971. (University microfilms 72-13269)
26. A. Tvarusko and L. S. Watkins, J. Electrochem. Soc. 118, 248 (1971).
27. C. W. Tobias, M. Eisenberg and C. R. Wilke, J. Electrochem. Soc. 99, 359C (1952).

28. N. Ibl and R. Muller, Z. Elektrochem. 59, 671 (1955).
29. C. S. Lin, R. W. Moulton and G. L. Putnam, Ind. Eng. Chem. 45, 640 (1953).
30. R. N. O'Brien, W. F. Yakymshyn and J. Leja, J. Electrochem. Soc. 110, 820 (1963).
31. K. W. Beach, R. H. Muller and C. W. Tobias, Rev. Sci, Instr. 43, 625 (1972).

FIGURE CAPTIONS

Fig. 1. Light deflection in a refractive index field due to local variations in refractive index n . A wave front W_1 , becomes tilted to W_2 after an increment of travel dx . The associated propagation direction N_1 , is changed to N_2 .

Fig. 2. Effect of the choice of focal plane on geometrical distortions due to light deflection in an electrolytic boundary layer.

(a) optics focused on light exit side of cell, (b) optics focused within cell (c) optics focused on light entrance side of cell (refraction at cell-air interface and in cell wall not shown).

A - electrolyte

B - electrode

C - deflected beam

D,K,L - virtual locations of electrode surface

E - auxiliary ray

F,F' - primary and secondary focal points of objective lens

G - objective lens

H - image of electrode surface

I - image plane

J - picture of electrode shadow

Fig. 3. Focusing in the absence of light deflection ; refraction in cell wall and at cell exit. E - real, immersed object, E' - virtual location of E, F - real plane of focus in cell, F' - virtual plane of focus (focus in air).

- Fig. 4. Focusing in the presence of light deflection; geometrical distortion. ABC - deflected light beam, F - real plane of focus, F' - virtual plane of focus, g - lateral displacement of virtual beam origin.
- Fig. 5. Light deflection in cathodic boundary layer; choice of plane of focus at light entrance side of cell. Overlapping beams are separated in the virtual plane of focus F'. (a) refractive index profile, (b) ray tracings.
- Fig. 6. Determination of the optical path length error (refractive index distortion) due to light deflection. Plane of focus at entrance of light into the medium of variable refractive index. AC - deflected beam, EI - undeflected reference beam, CI - equiphase circle.
- Fig. 7. Light deflection in anodic boundary layer. (a) Refractive index profile. (b) Absorbing electrode surface. Undeflected beam, outermost deflected beam which contributes to the image and absorbed beam. (c) Reflecting electrode surface. Unreflected, singly and doubly reflected beams.
- Fig. 8. (a) Refractive index profile in a cathodic boundary layer, (b) Numerical computation of a deflected light beam GL in a boundary layer. A,D - cell walls, B - electrolyte, C - electrode, P - equiphase circle centered in virtual beam origin E'.
- Fig. 9. Interference fringes (B) to (E) computed for refractive index profile (A) for different choices of the plane of focus. Cell width 1 cm, glass wall thickness 1.27 cm, cathodic current density 4 mA/cm^2 , abscissa - concentration with 0.04M CuSO_4 per vertical

division, increasing to the right (0 and 0.04 repeated at each vertical line). Ordinate - distance from interface in mm.

B - focus 3.4 mm inside glass wall farthest from the camera

C - focus on inside face of glass wall farthest from the camera

D - focus inside cell, 3.75 mm from the inside face of the glass wall farthest from the camera

E - focus inside cell, 7.5 mm as above

Fig. 10. Top: Effect of the choice of plane of focus on the appearance of the interferogram of a cathodic boundary layer. 0.1 M CuSO_4 solution, current density 5.0 ma/cm^2 ; cell thickness 1.0 cm; glass wall thickness 1.27 cm. The zero of the vertical scale defines the electrode shadow before the boundary layer was formed. Bottom: Cross-section of electrolytic cell with position of planes of focus (dashed lines) for interferograms a to d.

E - incoming collimated light

F - glass wall farthest from the camera

G - electrolyte and electrode

H - glass wall near the camera

J - camera lens

Fig. 11. Ray tracings on the cross section of an electrolytic cell (right) with a cathodic boundary layer (10 mA/cm^2). Width of cell and glass wall 10 and 12.7 mm, respectively. The concentration profile is shown by the top curve on the left (abscissa: molarity of copper sulfate in water). The bottom curve on the left shows the

interference fringe for a plane of focus on the inside of the glass wall farthest from the camera (choice B of Fig. 12).

Fig. 12. Lack of effect of glass wall thickness on interference pattern. Cathodic boundary layer for 10 mA/cm^2 current density.

A - concentration profile

B to E - computed interference fringes for different choices of the plane of focus given in the text.

Abcissa: copper sulfate concentration, 0.1M per division, increasing to the right (0 and 0.1 repeated at each vertical line)

Ordinate: distance (in mm) from image of electrode surface in the absence of light deflection

(a) - glass wall thickness 1.27 mm

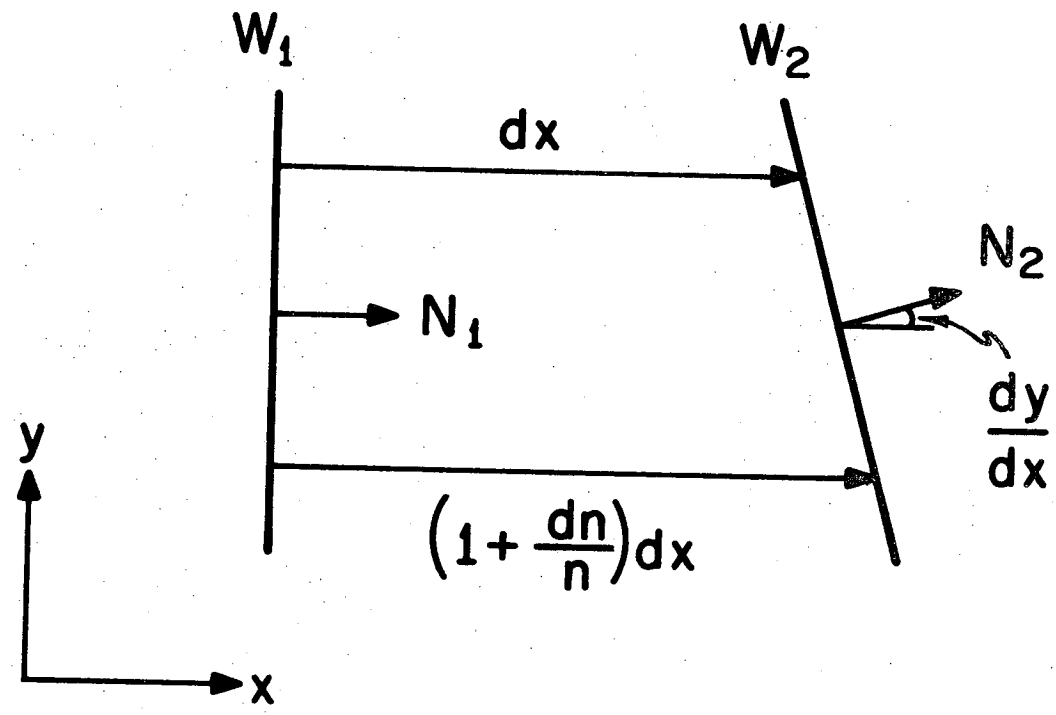
(b) - glass wall infinitely thin.

Fig. 13. Effect of cell misalignment on interference fringes of a cathodic boundary layer for different choices of the plane of focus. 10 mA/cm^2 , angle of incidence $+2.3^\circ$ (away from electrode face), other data as in Fig. 12.

Fig. 14. Effect of cell misalignment on interference fringe and ray tracings for a cathodic boundary layer. 7.5 mA/cm^2 , angle of incidence -2.3° (toward electrode face). Other data as in Fig. 11.

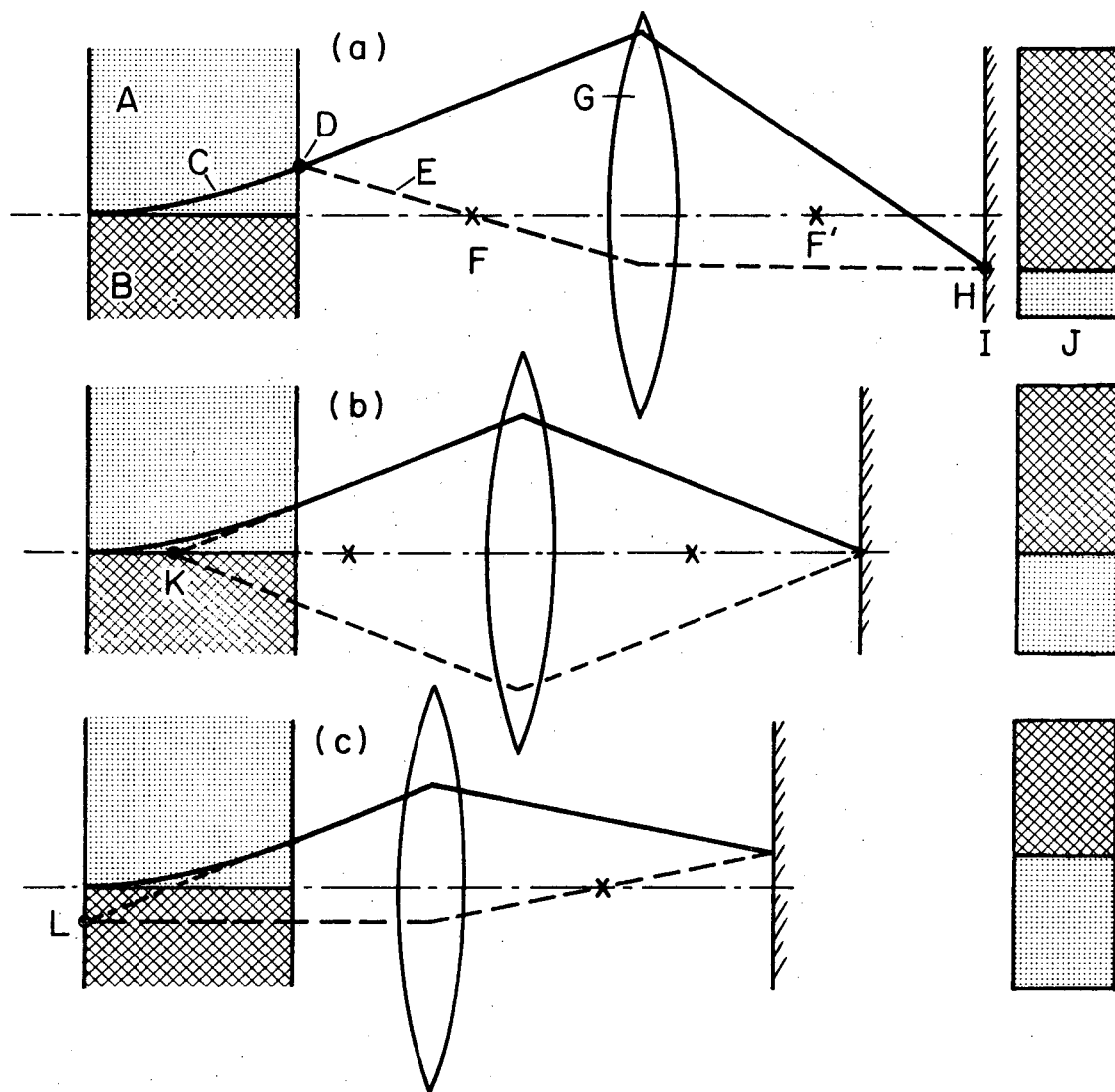
Fig. 15. Effect of the choice of plane of focus on interference fringes of an anodic boundary layer. 10 mA/cm^2 . Other data as in Fig. 12.

- Fig. 16. Effect of cell misalignment on interference fringes of an anodic boundary layer for different choices of the plane of focus. 10 mA/cm^2 , angle of incidence $+3.4^\circ$ (away from electrode face), other data as in Fig. 12.
- Fig. 17. Interference fringes of a liquid junction between 0 and 0.1M copper sulfate for different choices of the plane of focus. Other data as in Fig. 12.
- Fig. 18. Effect of cell misalignment on the interference fringes of the liquid junction of Fig. 17. Angle of incidence -2.3° (toward electrode face).
- Fig. 19. Interference fringes of a concentration minimum for different choices of the plane of focus. Other data as in Fig. 12.
- Fig. 20. Interference fringes of a concentration maximum for different choices of the plane of focus. Other data as in Fig. 12.



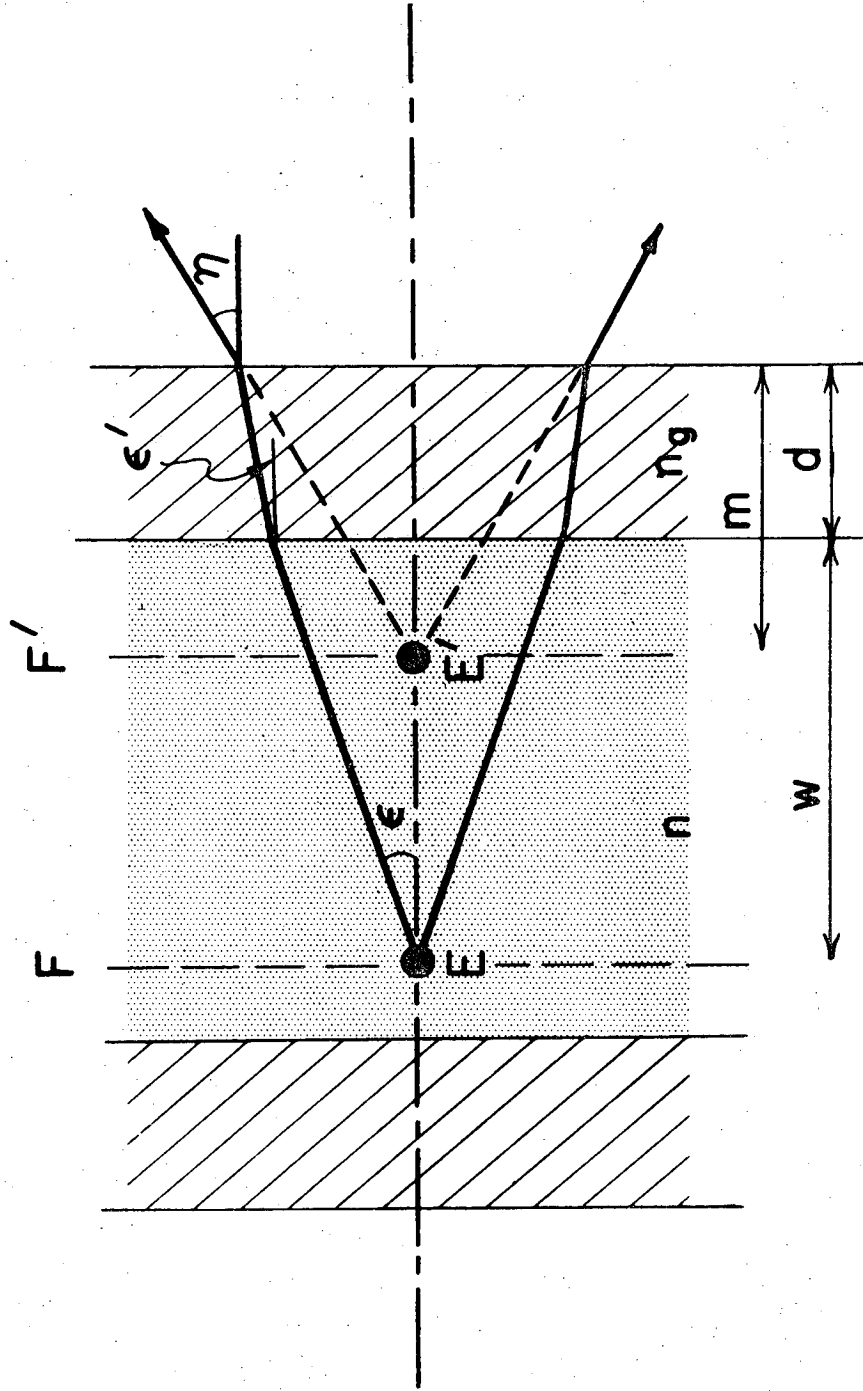
XBL729-4036

Fig. 1



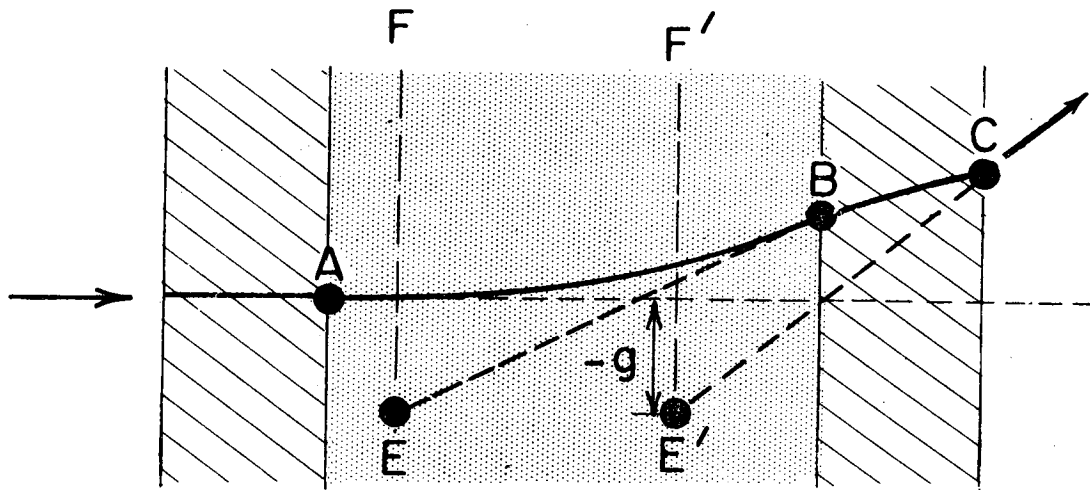
XBL697-3200

Fig. 2



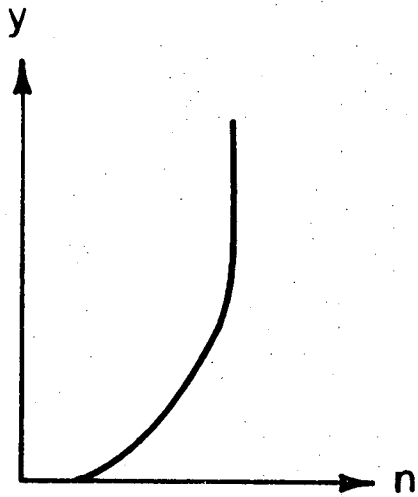
XBL723-2546

Fig. 3

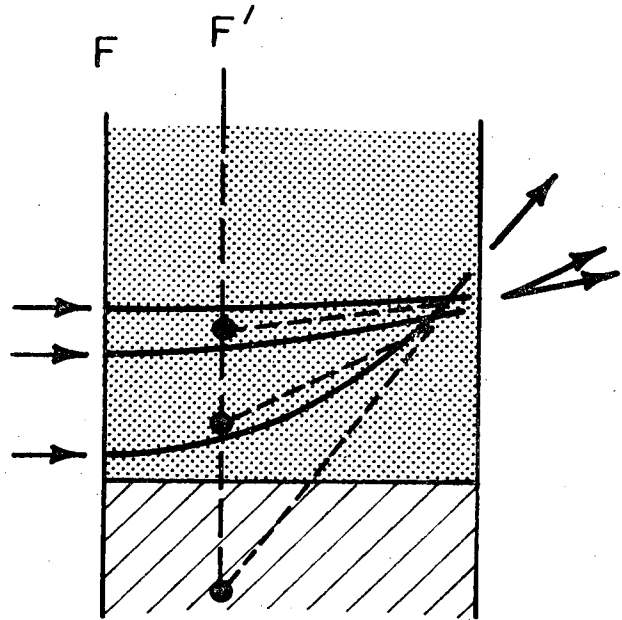


XBL 727 - 2550B

Fig. 4



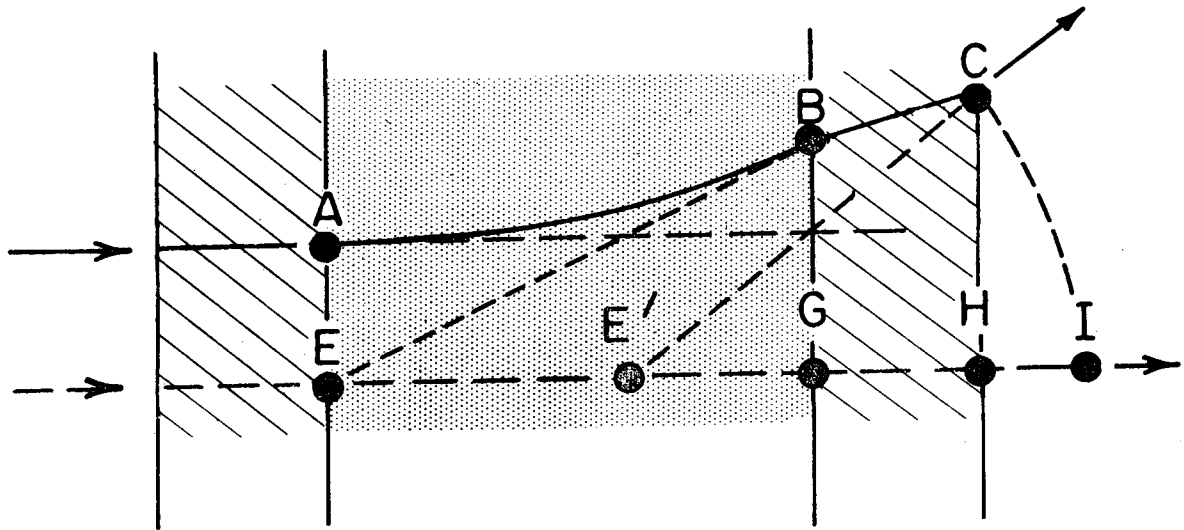
(a)



(b)

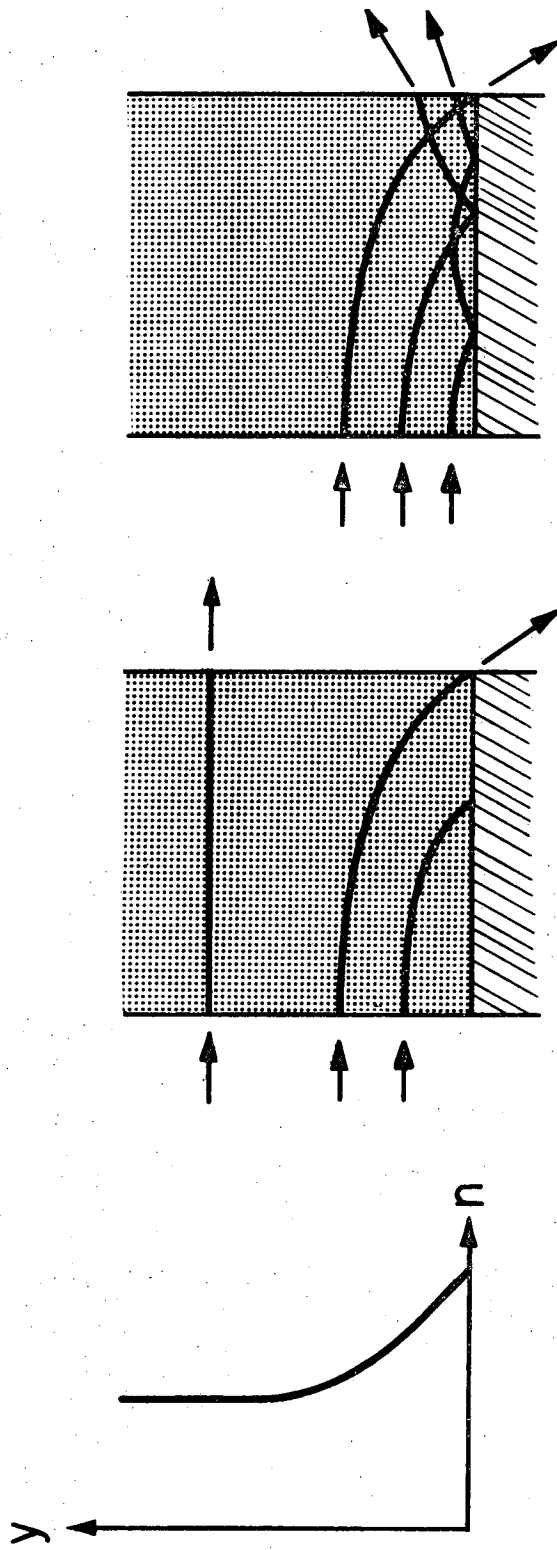
XBL727-3420

Fig. 5



XBL727 -2548B

Fig. 6



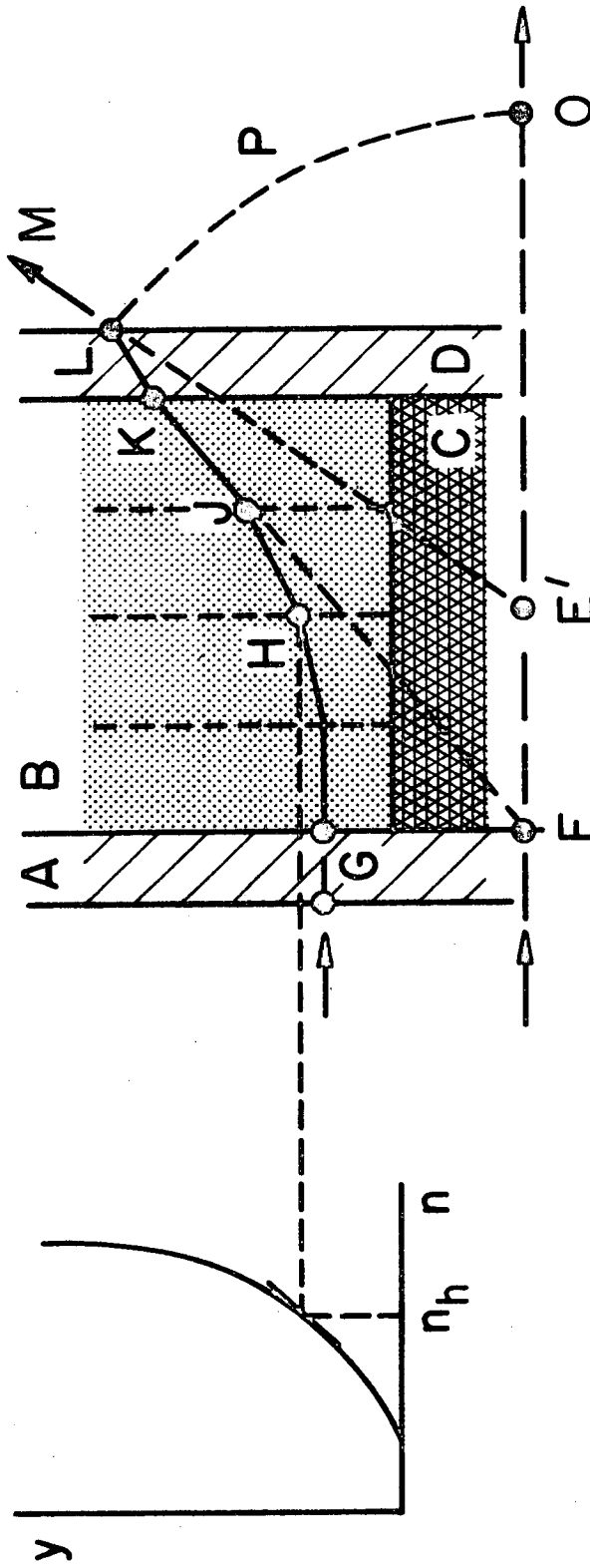
(c)

(b)

(a)

XBL717-3962A

Fig. 7



(a)

(b)

XBL729-4035

Fig. 8

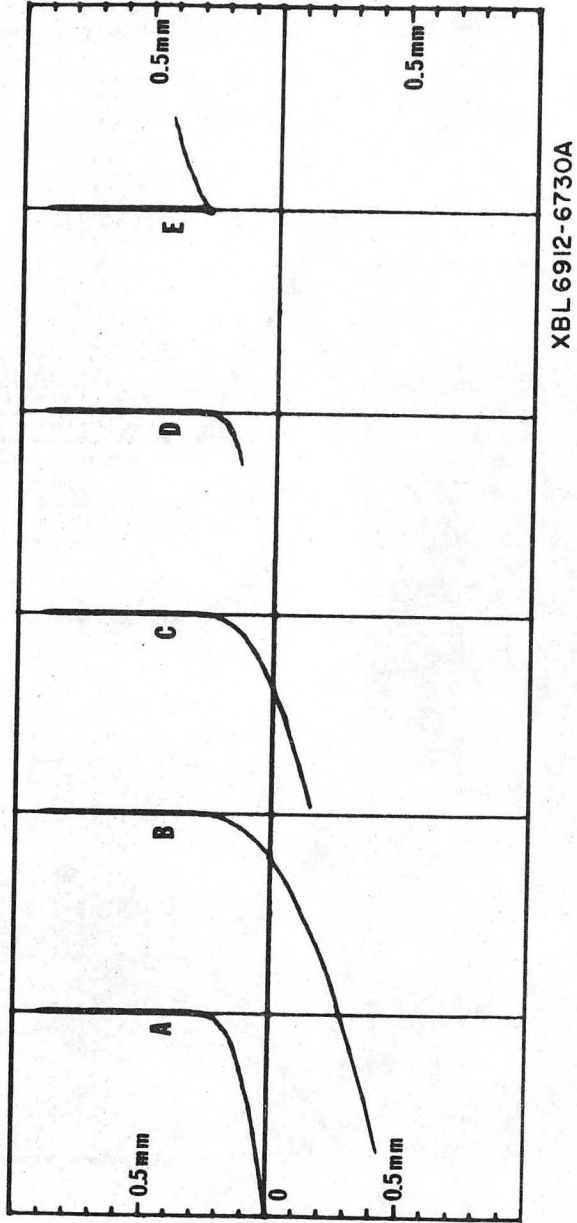
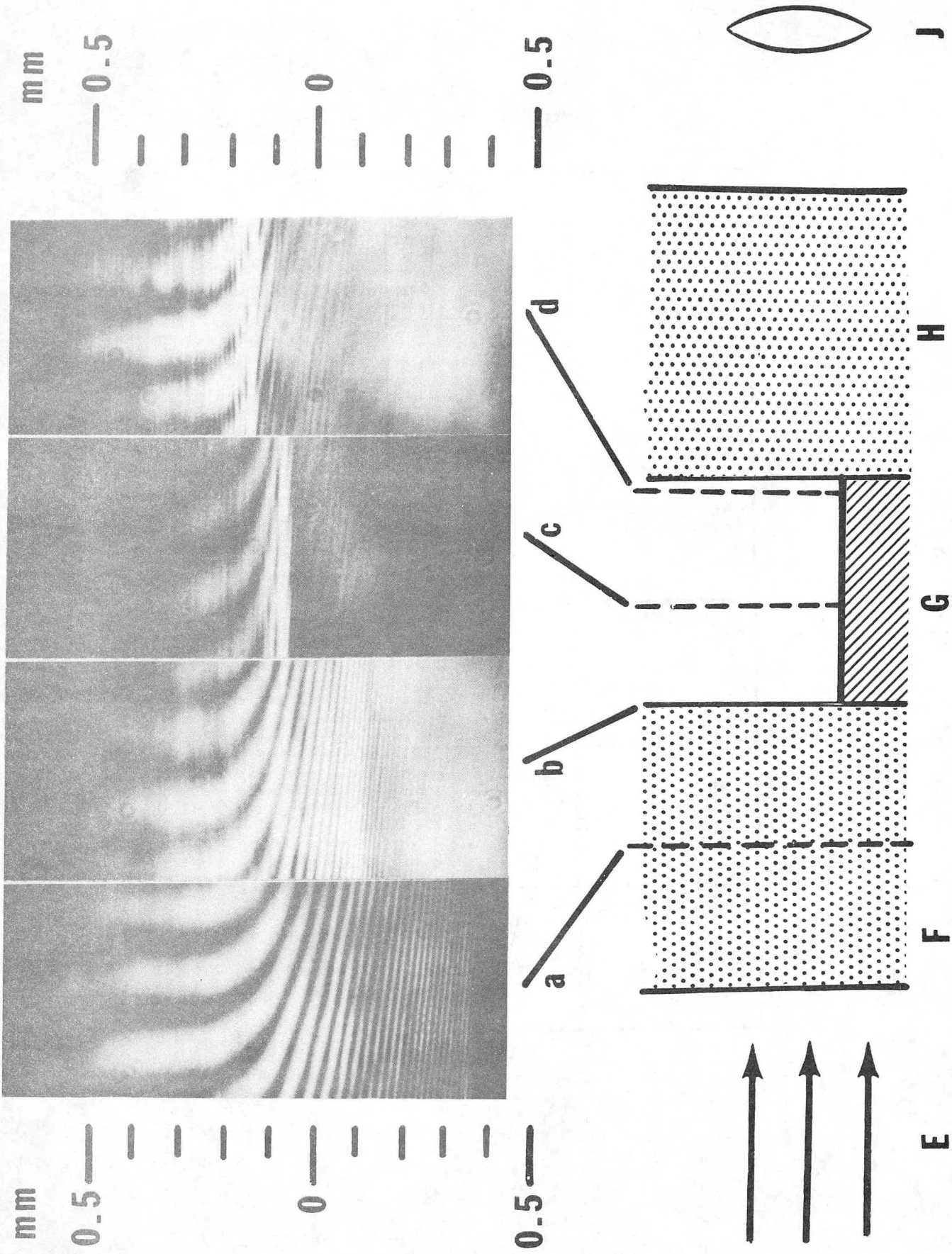
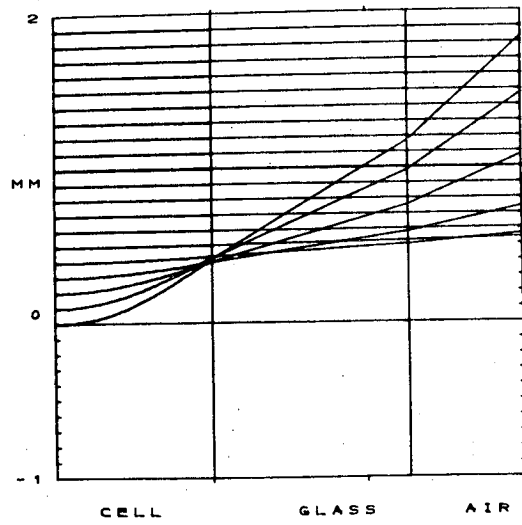
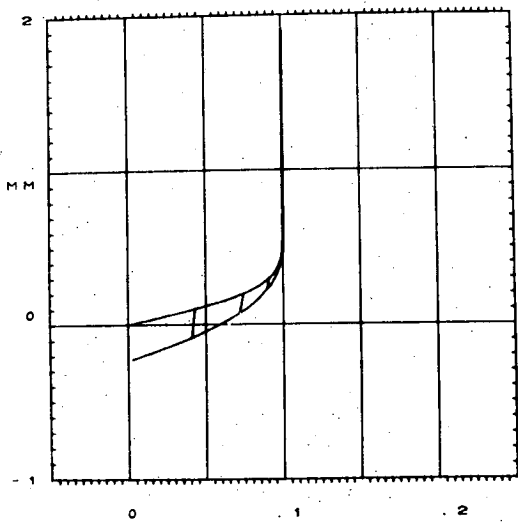


Fig. 9



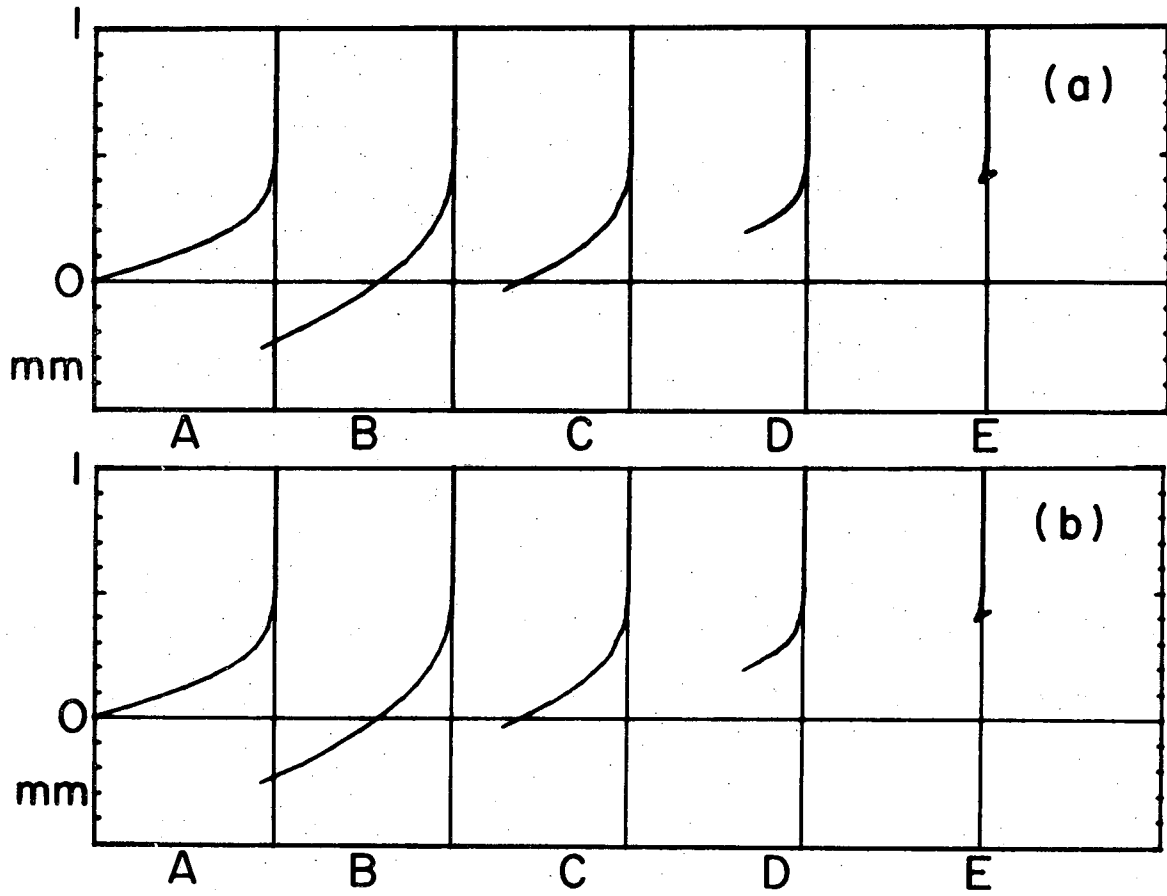
XBB 697-4914A

Fig. 10



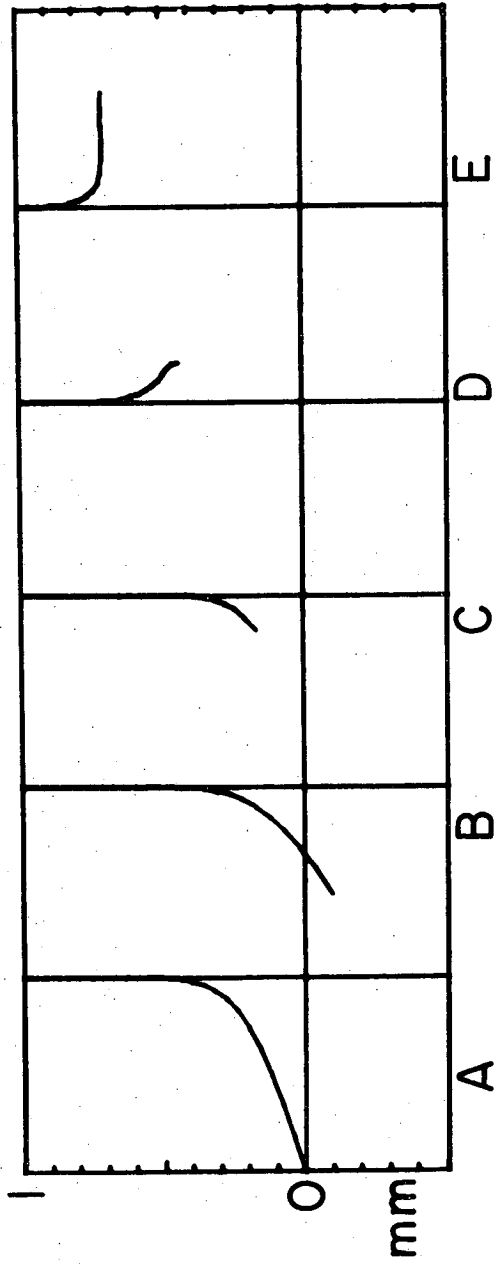
XBL 7012-7193

Fig. 11



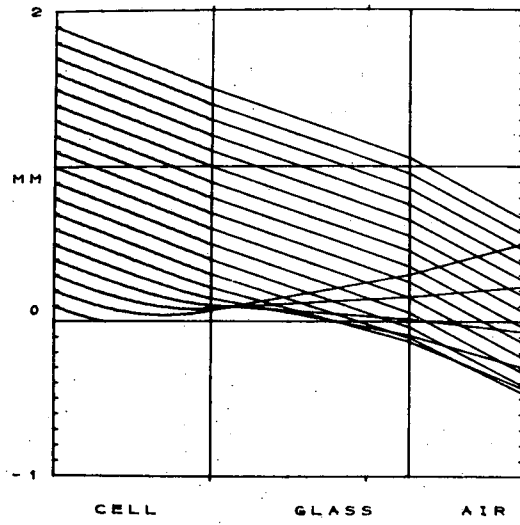
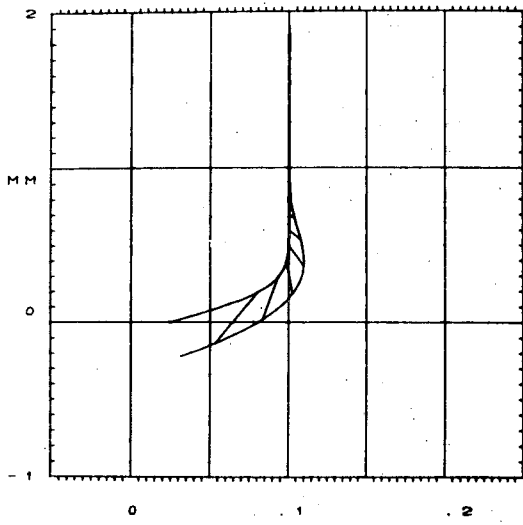
XBL729-4057

Fig. 12



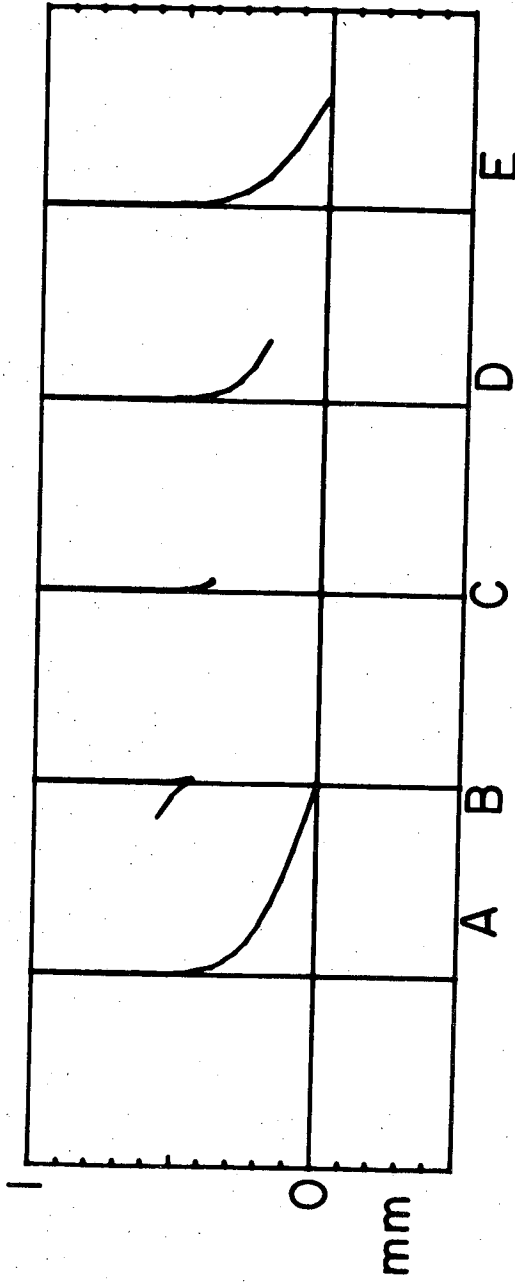
XBL7012-7210A

Fig. 13



XBL 7012-7191

Fig. 14



XBL7012-7217A

Fig. 15

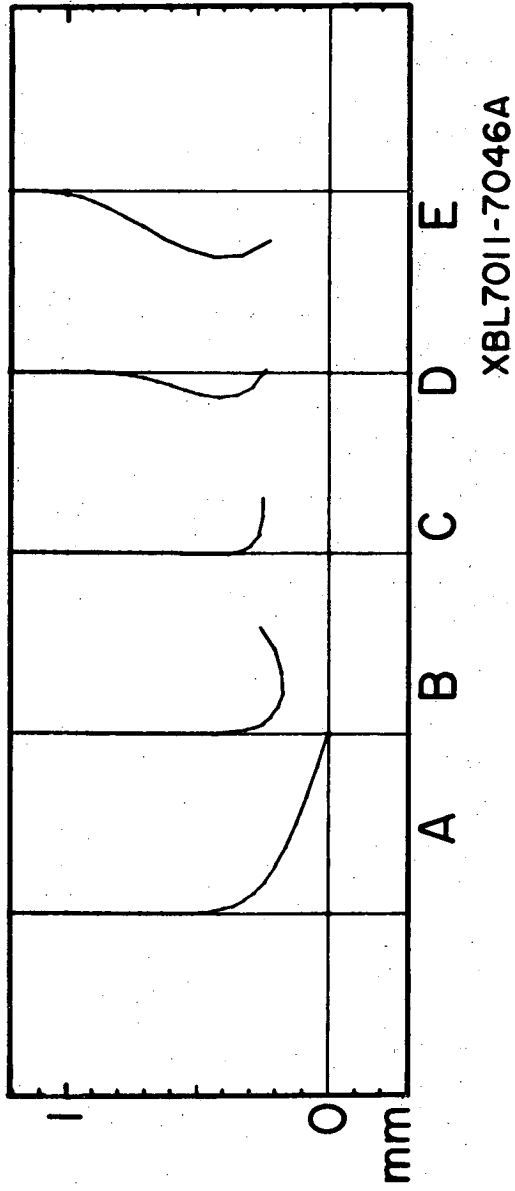


Fig. 16

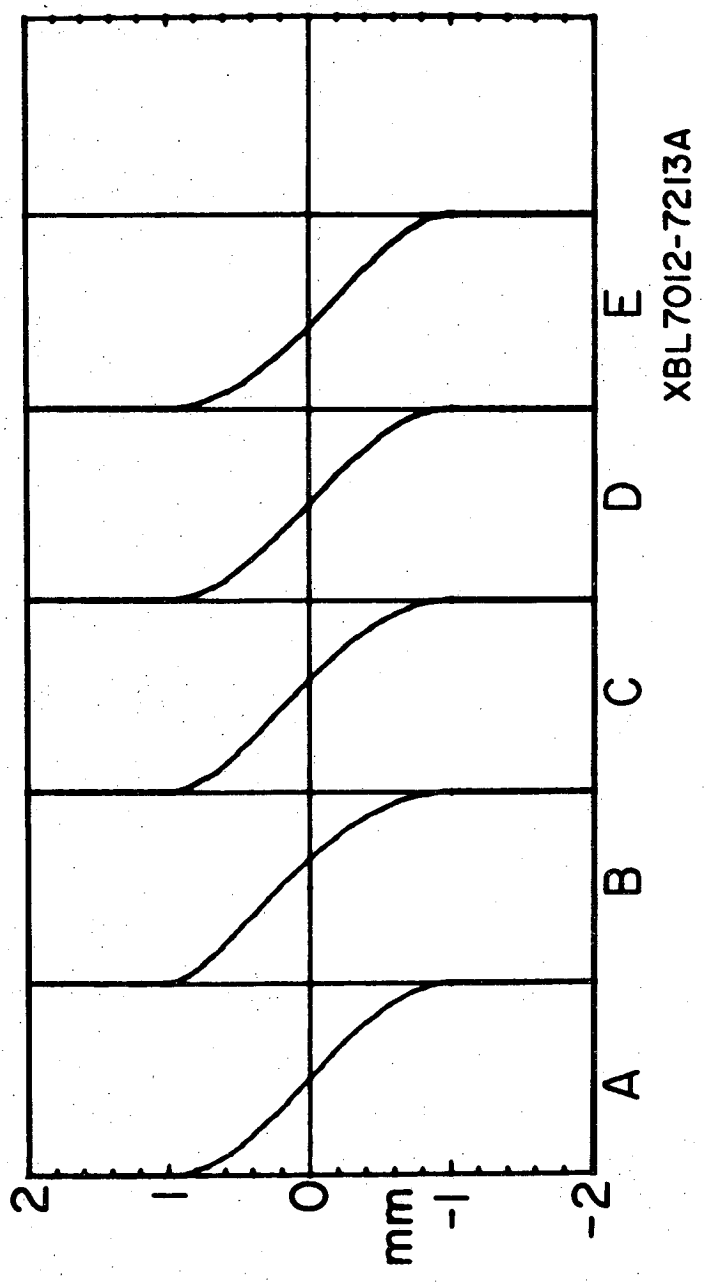
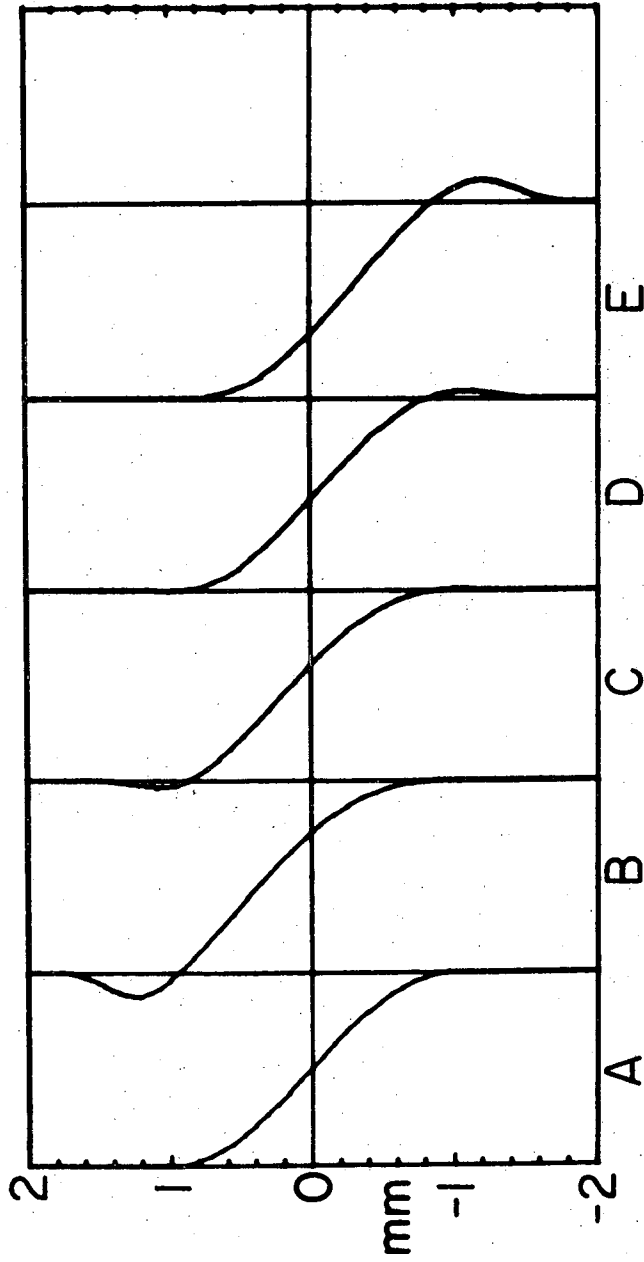
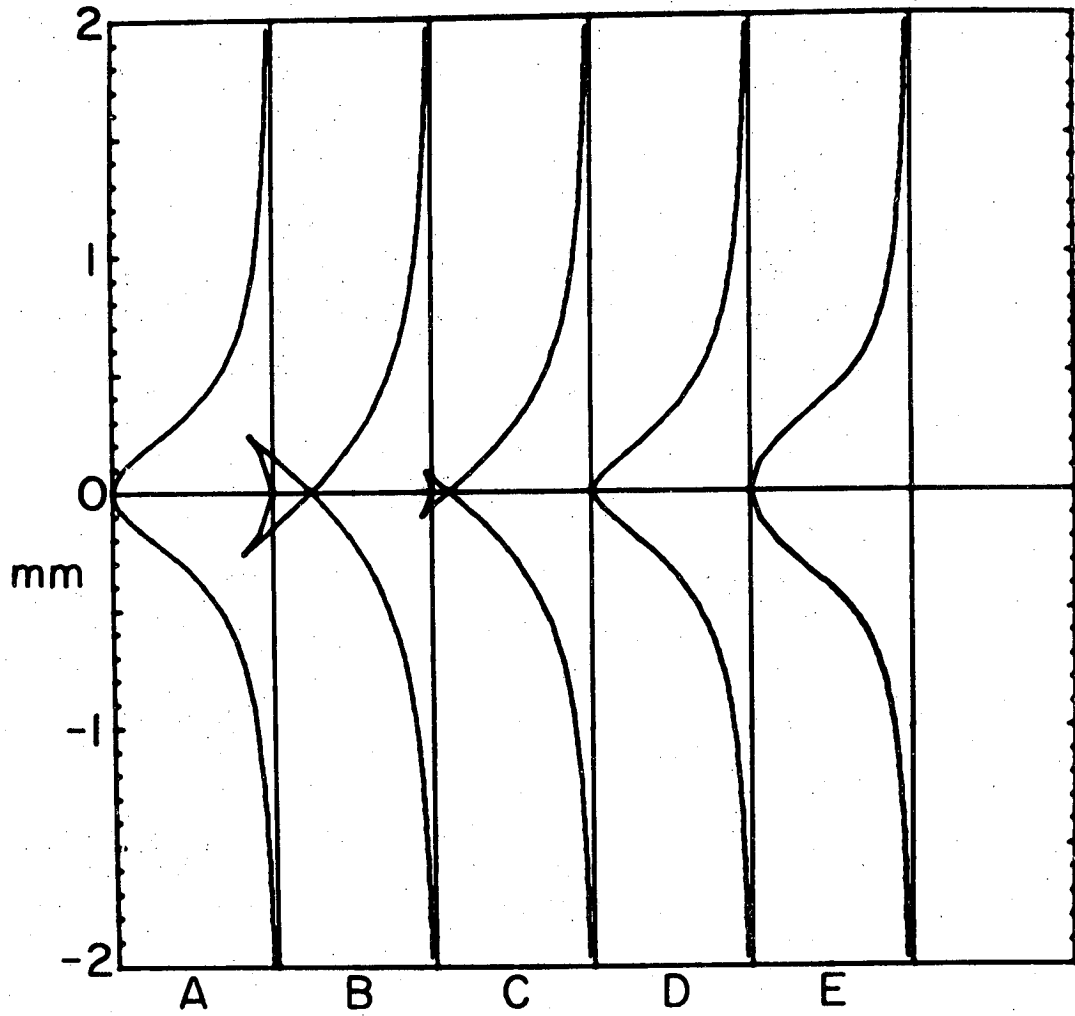


Fig. 17



XBL7012-7214A

Fig. 18



XBL7011-7041-A

Fig. 19

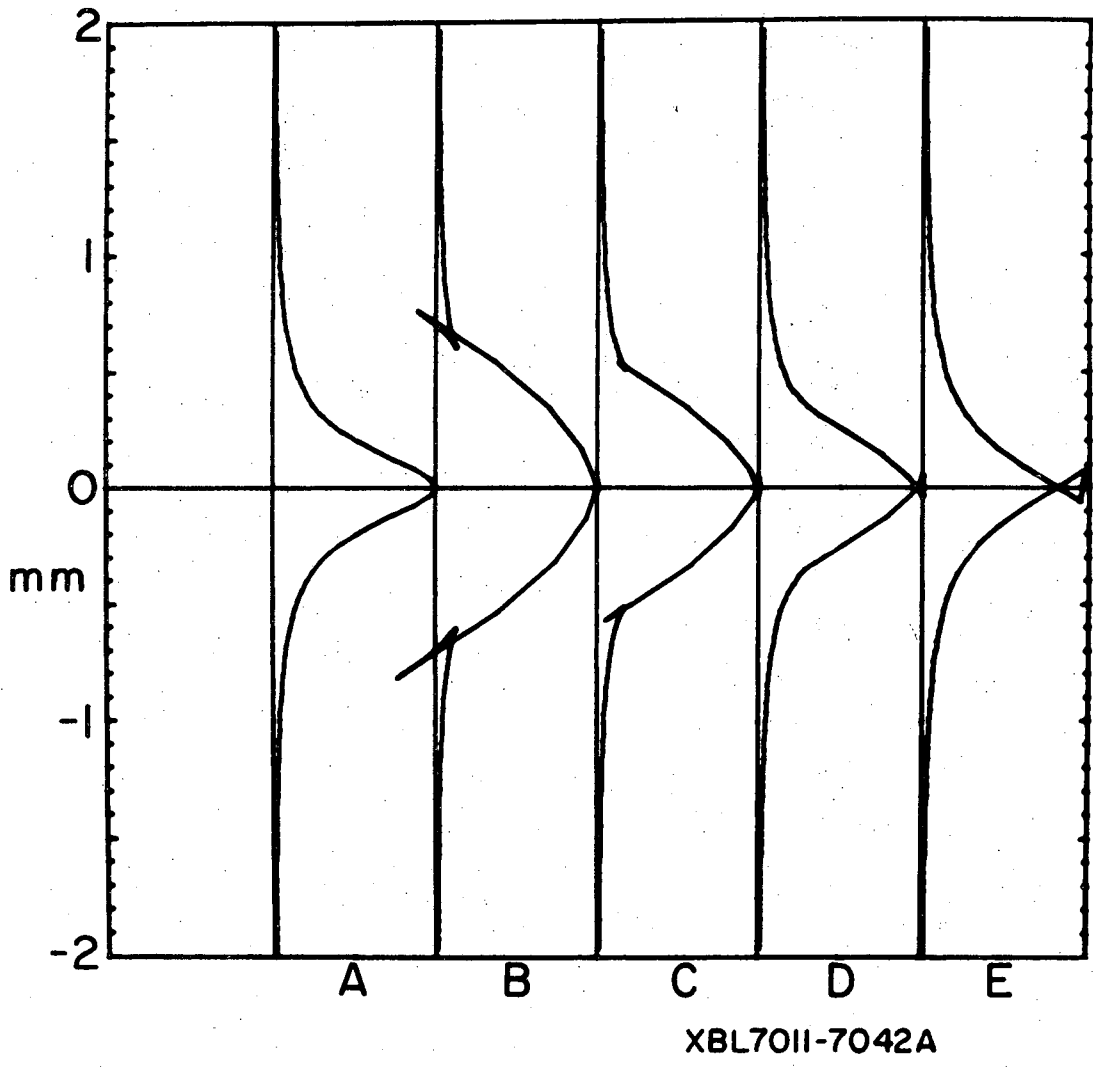


Fig. 20

LEGAL NOTICE

This report was prepared as an account of work sponsored by the United States Government. Neither the United States nor the United States Atomic Energy Commission, nor any of their employees, nor any of their contractors, subcontractors, or their employees, makes any warranty, express or implied, or assumes any legal liability or responsibility for the accuracy, completeness or usefulness of any information, apparatus, product or process disclosed, or represents that its use would not infringe privately owned rights.

TECHNICAL INFORMATION DIVISION
LAWRENCE BERKELEY LABORATORY
UNIVERSITY OF CALIFORNIA
BERKELEY, CALIFORNIA 94720